

# Towards engineering artificial graphene

L. Nádorník,<sup>1,2,\*</sup> M. Orlita,<sup>3,2,1</sup> N. A. Goncharuk,<sup>2</sup> L. Smrčka,<sup>2</sup> V. Novák,<sup>2</sup> V. Jurka,<sup>2</sup>  
K. Hruška,<sup>2</sup> Z. Výborný,<sup>2</sup> Z. R. Wasilewski,<sup>4</sup> M. Potemski,<sup>3</sup> and K. Výborný<sup>2,5</sup>

<sup>1</sup>*Faculty of Mathematics and Physics, Charles University, Ke Karlovu 3, 121 16 Praha 2, Czech republic*

<sup>2</sup>*Institute of Physics, ASCR, v.v.i., Cukrovarnická 10, 162 53 Praha 6, Czech Republic*

<sup>3</sup>*Laboratoire National des Champs Magnétiques Intenses,  
CNRS-UJF-UPS-INSA, 25, avenue des Martyrs, 38042 Grenoble, France*

<sup>4</sup>*Institute for Microstructural Sciences, NRC, Ottawa, Ontario, Canada K1A 0R6*

<sup>5</sup>*Department of Physics, State University of New York at Buffalo, New York 142 60, USA*

We report on a measured non-linear in magnetic field dependence of cyclotron resonance absorption as well as its splitting into several modes in GaAs/Al<sub>x</sub>Ga<sub>1-x</sub>As heterostructures with an etched hexagonal lateral superlattice, i.e., in artificial graphene. Our explanation, based on the perturbation theory, describes the observed phenomena as a weak effect of the lateral potential on the two-dimensional electron gas (2DEG). In addition, we propose a set of four criteria that one has to satisfy to realize graphene-like physics in materials containing 2DEG with a tunable hexagonal modulation.

PACS numbers: 73.22.Pr, 73.21.Cd, 78.67.Pt

## I. INTRODUCTION

The range of paths to explore Dirac fermions has recently been (once again) extended beyond the standard field of graphene<sup>1,2</sup> to a completely new class of systems. The artificial graphene (AG) concept is based on the idea of creating massless fermions in semiconductor heterostructures by modulating the two-dimensional electron gas (2DEG) with a lithographically created superlattice. If the introduced potential reflects the hexagonal symmetry of natural graphene and it is strong enough, the electronic structure changes towards a graphene-like one.<sup>3,4</sup> A lateral modulation of the surface by etching<sup>5-7</sup> or by placing a gate electrode represent two possible techniques. Lithographical fabrication offers more freedom in creating artificial crystals than preparation of structures from real atoms and consequently the electronic properties of the AG, such as the slope of the Dirac cone (that is the Fermi velocity), can be widely tuned.<sup>8</sup> Moreover, various proof-of-principle device prototypes<sup>9</sup> (filters, valves,<sup>10</sup> Veselago lens,<sup>11</sup> splitters<sup>12</sup> etc.) could be more easily tested on AG basis owing to the larger versatility of electron beam lithography compared to an atom-by-atom manipulation required for fabrication of natural graphene devices. In the present work, with help of a simplified AG model, we first formulate four basic criteria to make graphene-like characteristics observable and then show how they can be tested using magneto-optical experiments. We conclude that AG with the desired hallmarks of Dirac-fermions may be technologically attainable but their actual observation is missing so far.

## II. THEORY

Compared to previous works,<sup>4,8</sup> we use a simplified AG model that allows for a better insight into how the individual parameters of the modulation potential  $V(\vec{r})$ ,

$\vec{r} = (x, y)$  govern the miniband structure. We consider  $V$  comprising of three cosine functions

$$V(\vec{r}) = V_0(\cos \vec{g}_1 \vec{r} + \cos \vec{g}_2 \vec{r} + \cos \vec{g}_3 \vec{r}), \quad (1)$$

where  $\vec{g}_1 = 2\pi/a(1/\sqrt{3}, 1)$ ,  $\vec{g}_2 = 2\pi/a(2/\sqrt{3}, 0)$ ,  $\vec{g}_3 = \vec{g}_2 - \vec{g}_1$  are the basis-vectors of the graphene reciprocal space,  $a$  is the distance between two minima of the applied potential [Fig. 1(a)] and  $V_0$  is the potential amplitude. If we construct the Hamiltonian matrix in basis  $\mathcal{B}$  of plain waves,

$$\mathcal{B} = \left\{ e^{i(\vec{k} + \vec{K}_{n_1 n_2}) \vec{r}}, \vec{K}_{n_1 n_2} = n_1 \vec{g}_1 + n_2 \vec{g}_2 \right\}, \quad (2)$$

the ratio of diagonal to off-diagonal matrix elements is determined by  $V_0$  and  $a$ . Except for an overall scaling, the eigenvalues depend on a single dimensionless parameter

$$\zeta = \frac{m^*}{\hbar^2} V_0 a^2, \quad (3)$$

where  $m^*$  is the electron effective mass (in GaAs, 0.067 of the electron vacuum mass  $m_0$ ). Up to a factor of the order of unity, it is  $\zeta \simeq V_0/E_0$  where  $E_0$  is the kinetic energy of a free electron at the  $K$ -point of the Brillouin zone.

Depending on  $\zeta$ , we obtain miniband spectra continuously varying from the free 2DEG, through nearly-free and tight-binding models, up to completely flat bands corresponding to isolated (artificial) atoms. We point out that *two* Dirac cones can be found (within the lowest six minibands, see Fig. 2(b),(c) with Fermi velocities  $v_F = 2.4 \times 10^4$  and  $4.8 \times 10^4$  m.s<sup>-1</sup> when  $a = 200$  nm. Both Dirac cones were numerically explored and their Dirac-fermion-like nature was confirmed in terms of spectral properties (cone-like character with trigonal warping) and wavefunctions.<sup>4</sup> Maximum Dirac cones size is of the order of  $E_0$ . Further quantitative studies of the

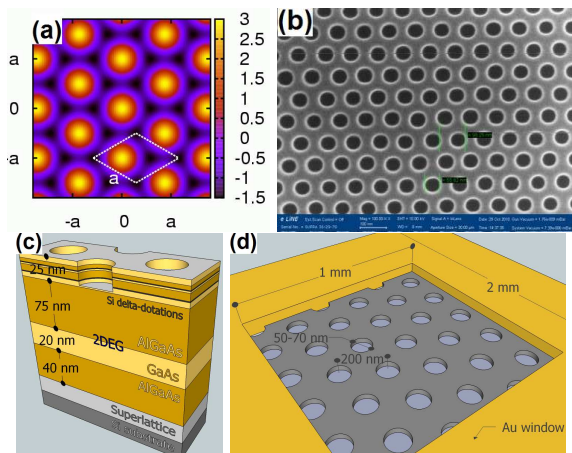


FIG. 1. (color online) Artificial graphene: Part (a): hexagonal potential of Eq. (1) defining the AG (in units of  $V_0$ ). Dark regions correspond to “atom positions” in the real graphene; the primitive cell is indicated. (b): Scanning electron microscope image of the surface of one of the samples, (c): its atomic layer structure (ZDEG depth  $\approx 100$  nm) and (d): the sample layout (not at scale).

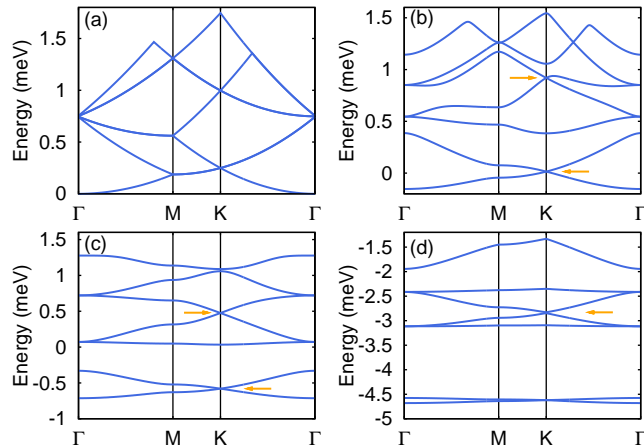


FIG. 2. (color online) Minibands generated for several values of the parameter  $\zeta$ . (a):  $\zeta = 0$ , dispersion of a free 2DEG. (b):  $\zeta = 0.3$ , first Dirac cones develops (indicated by arrow), the second one appears but remains covered by other bands. (c):  $\zeta = 0.9$ , both Dirac cones fully develop. (d):  $\zeta = 4.0$ , tight-binding type narrow minibands form and Dirac cones gradually flatten, ultimately becoming again unobservable. For  $a = 200$  nm, a,b,c, and d correspond to  $V_0 = 0, 0.4, 1$  and  $4$  meV in GaAs.

Dirac cones characteristics seem of less use with regard to the simplicity of the model; in the following we show how it, nevertheless, can be employed as a guide for AG fabrication.

Four criteria shall now be stated necessary to observation of graphene-like physics in AG. (i) *Suitable miniband structure* — looking at Fig. 2, the obvious first criterion is to appropriately adjust the  $\zeta$  parameter lest the de-

sired Dirac cones be not “covered” by other branches of the miniband structure. For the second Dirac cone, we find the range  $0.5 < \zeta < 4.0$  corresponding to  $V_0$  between  $0.6$  and  $4.5$  meV (for  $a = 200$  nm as in our samples described below). (ii) *Fermi level positioning* — to observe graphene-like properties, the Fermi level,  $E_F$ , should cross the linear part of the spectrum. Estimated values of  $E_F$  for the first and second Dirac cones for  $\zeta = 0.9$  are  $0.15$  and  $1.2$  meV approximately corresponding to carrier concentrations  $n \approx 0.5 \times 10^{10}$  and  $3.3 \times 10^{10}$   $\text{cm}^{-2}$ , respectively, and for  $\zeta = 4$  then  $n \approx 6 \times 10^{10}$   $\text{cm}^{-2}$  (see Appendix A), suggesting that the second Dirac cone would be better accessible from technological point of view. Although the first Dirac cone develops already for smaller  $V_0$  it would force the experimentalist to work at too low  $n$ . If  $a$  is reduced with  $\zeta$  remaining the same, the system offers somehow more favourable perspectives:  $\zeta = 0.9$ ,  $V_0 = 4$  meV and  $a = 100$  nm implies  $n \approx 1.7 \times 10^{10}$  and  $n \approx 1.4 \times 10^{11}$   $\text{cm}^{-2}$ , for the first and second Dirac cone, and the identical shape of minibands (including the Dirac cones) as in Fig. 2(c), only moved to higher energies. (iii) *Low disorder* — the idealized miniband structure, as suggested in Fig. 2, will be smeared by various irregularities of the system: both by impurities present in the unmodulated heterostructure and imperfections of the modulation potential. The minimal requirement to meet is that the mean free path  $l_e = \hbar\mu\sqrt{2\pi n}/e^2 \gg a$ . This criterion is not too stringent since  $l_e \approx 500$  nm for  $\mu = 10^5$   $\text{cm}^2/(\text{V}\cdot\text{s})$  and  $n = 10^{11}$   $\text{cm}^{-2}$  but it only constitutes a necessary and not a sufficient condition for tracing AG physics. (iv) *Careful probing* — the last important aspect is that the measurement conditions must not affect too strongly the AG system. Typically, this means that both the temperature,  $T$ , and magnetic field,  $B$ , are low enough. To preserve graphene-like behaviour, the system has to be governed by the modulation potential, and the cyclotron quantization has to play only the role of a scanning means. Hence,  $\hbar\omega_c \ll E_{DC}$  with  $E_{DC}$  denoting the Dirac cone size in energy, and since the cyclotron energy  $\hbar\omega_c = \hbar eB/m^*$  equals  $\sim 1.7$  meV at  $B = 1$  T, the quest for Dirac fermions in AG should aim at relatively weak magnetic field. Miniband structures in Fig. 2 show  $E_{DC} \sim 0.3$  meV (note that a good general estimate of  $E_{DC}$  is  $E_0$ ) therefore tolerable magnetic fields are hundreds of mT at the most. Similarly, to keep  $kT \ll \hbar\omega_c$ , temperatures in sub-kelvin range may be needed.

### III. EXPERIMENT

To create the required type of potential on the surface of our samples, we fabricated a pattern formed by holes in triangular symmetry, etched into material. Electron beam lithography and dry etching processes ( $\text{Ar}^+ + \text{SiCl}_4$ ) were used to obtain the three samples under study (A, B and C, see Table I) which have holes etched to 15-25, 20 and 48 nm in depth. The diameter of

holes was always 50-70 nm and nearest-neighbour distance  $a = 200$  nm. Two types of GaAs/AlGaAs heterostructures have been used as a starting material: the first one for the samples A and B, containing a 100 nm deep 2DEG formed in the 20 nm wide quantum well and charged by two Si delta-doped layers, 14 nm and 24 nm under the surface (Fig. 1(c)); the second one for the sample C, which consists of the 115 nm deep 2DEG confined in a triangular quantum well under one 50 nm wide Si-doped layer. Modulated areas were covered by a 50 nm thin layer of gold with a  $1 \times 1$  mm<sup>2</sup> window [Fig. 1(d)].

The samples were placed into a helium-pumped cryostat at  $T = 2$  K, equipped with a superconducting coil producing the magnetic field up to 13 T. The Fourier transform spectrometer working down to photon energies of  $\hbar\omega \approx 4$  meV, with a globar and mercury lamp as the radiation sources, was coupled to the cryostat. The signal was detected using bolometer kept at  $T = 2$  K. Transmission spectra have been collected with resolutions down to 0.125 meV. The initial concentration of carriers in samples before processing was changed as a result of etching as well as of illumination by visible parts of globar/mercury lamp emission spectra. Therefore, the actual concentration has been finally estimated from area of CR peak as  $n_{A,B} \sim 0.8 \times 10^{11}$  cm<sup>-2</sup> and  $n_C \sim 1.8 \times 10^{11}$  cm<sup>-2</sup> (see Appendix A for details). The carrier mobility after processing was estimated to be somewhat in excess of  $10^5$  cm<sup>2</sup>/(V.s) for all three samples and similar mobilities were inferred also from magneto-transport measurements on samples parent to C.

The electronic bands in our samples have been studied using methods of Landau level (LL) spectroscopy in far infrared spectral range. The magneto-transmission spectra of a set of three patterned samples and one reference sample have been measured. In Fig. 3, typical spectra, i.e., the transmission of the samples normalized to the response at  $B = 0$ , are presented for fields  $B = 3 - 7.5$  T. Transmission spectrum measured on the reference sample (an unpatterned wafer, the same as used for samples A and B) exhibited only a single cyclotron-resonance (CR) mode of the Lorentzian shape having energy of  $\hbar\omega_c$ . As shown in Figs. 3a-c, the transmission spectra measured on the patterned samples exhibit double- or multi-mode CR response at low magnetic fields. Characteristically, these additional modes appears at energies above  $\hbar\omega_c$ . This splitting of the CR mode into more components vanishes with the increasing  $B$ , but at different fields in different samples, i.e., this splitting depends on the strength of the modulation potential or the depth of etched holes. For stronger modulation potential (deeper holes), the multi-mode CR is visible up to higher magnetic fields (see Fig. 4).

## INTERPRETATION

The question raised now is what we can learn from present experiment and whether signatures of Dirac

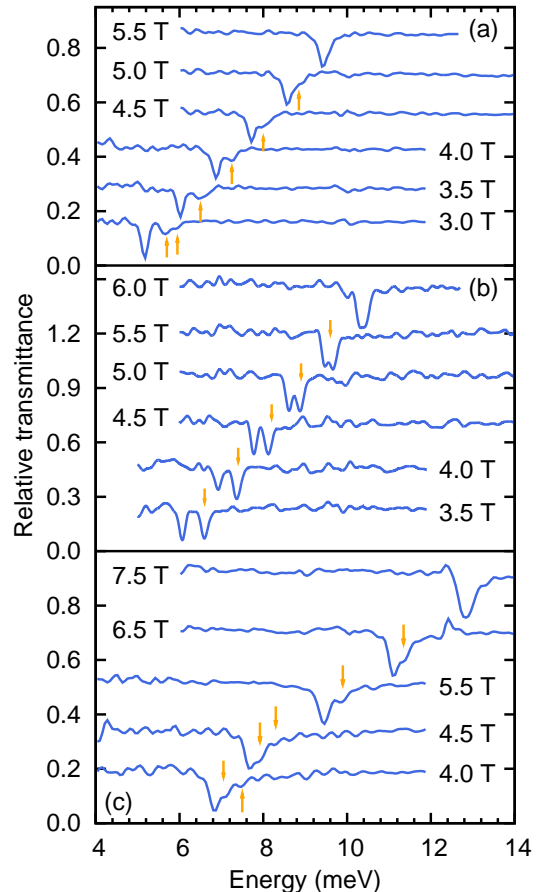


FIG. 3. (color online) Relative magneto-transmission spectra of studied samples A ( $d_{\text{holes}} \approx 15 - 25$  nm,  $d_{2\text{DEG}} = 100$  nm), B ( $d_{\text{holes}} = 20$  nm,  $d_{2\text{DEG}} = 100$  nm) and C ( $d_{\text{holes}} = 48$  nm,  $d_{2\text{DEG}} = 115$  nm) in parts (a), (b) and (c), respectively. The multi-mode character of cyclotron resonance absorption vanishes with the increasing magnetic field at  $B \approx 5, 6$  and  $7$  T in the sample A, B and C, respectively. All spectra are shifted vertically for clarity.

bands have been observed or how far are we from their observation. As can be seen in Fig. 3, the patterned structures show noticeably modified spectra, but observed changes are not as dramatic as we could, even intuitively, expect in case of a clear formation of Dirac-like electronic bands. The modulation potential seems to be not strong enough to incite Bloch waves mimicking Dirac-fermion physics. Main absorption features still occur close to  $\hbar\omega_c$  but in contrast to the cyclotron peak of the unmodulated 2DEG, they exhibit internal structure which disappears roughly as  $1/B$  (see Fig. 4) in the limit of high magnetic fields. Such behavior is suggestive of a perturbative effect of a potential whose strength becomes gradually weaker relative to the spacing of LLs. This spacing, the cyclotron energy  $\hbar\omega_c$ , then provides the dominant energy scale and the modulation potential  $V_0$  is only a perturbation described by the small parameter  $V_0/\hbar\omega_c$ . Data

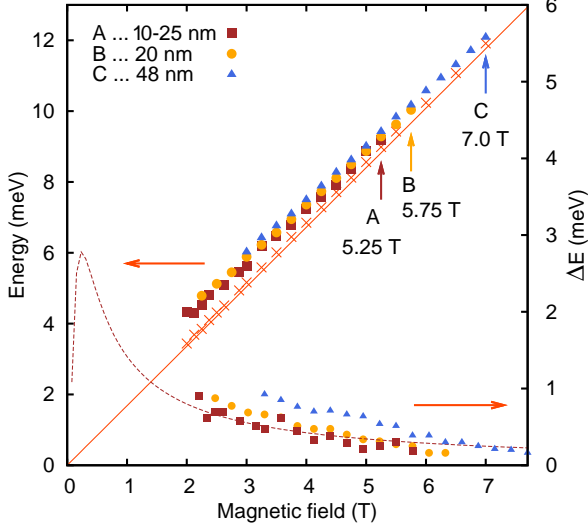


FIG. 4. (color online) Fanchart of transitions observed in studied specimens A, B and C, cf. Fig. 3 (left vertical axis): Vertical arrows depict magnetic fields at which the multi-mode character of CR absorption vanishes. The position of the main CR peak in spectra taken on the sample A is marked by crosses. The straight line corresponds to the theoretical CR-line position with an effective mass of  $m^* = 0.067m_0$ , which has been derived from measurements on reference (un-patterned) sample (not shown in this paper). Lower part of the figure (right vertical axis) shows derived values of CR-line splitting  $\Delta E$ . The dashed line corresponds to the fit of  $\Delta E$  for the sample A based on the theoretical model discussed in the text.

presented in Fig. 3 therefore bear witness to an overly strong effect of magnetic field that almost washes up the effect of the modulation potential and, similar to previous works, e.g., Ref. 8, we fail to observe graphene-like behavior on grounds of violating the forth criterion (as defined in Sec. II).

To remedy this shortcoming, measurements at lower magnetic fields are needed. This is in principle possible yet beyond the low-energy limit of the employed Fourier transform spectroscopy. Still, we can draw conclusions from our experiments regarding the first two criteria described in Sec. II. This way we first find how our samples need to be optimized in the future and second, what maximum magnetic fields can be employed for studying the projected graphene features. According to the first-order perturbation approach,<sup>14</sup> the unperturbed energies  $E_n = \hbar\omega_c(n + 1/2)$  are broadened into bands

$$E_{n,\kappa_x,\kappa_y} = E_n + V_0 e^{-2\beta^2/3} L_n(4\beta^2/3) \times \left\{ 2 \cos \beta^2 \left( \kappa_x + \frac{1}{\sqrt{3}} \right) \cos \frac{\beta^2 \kappa_y}{\sqrt{3}} + \cos \frac{2\beta^2 \kappa_y}{\sqrt{3}} \right\} \quad (4)$$

where  $\beta^2 = 2\pi^2 \ell_0^2 / a^2$ ,  $\ell_0^2 = \hbar / eB$  and  $\vec{\kappa}$  belongs to the hexagonal first magnetic Brillouin zone. Owing to special properties of Laguerre polynomials  $L_n$ ,<sup>15</sup> optical transition energies, that are  $E_{n+1,\kappa_x,\kappa_y} - E_{n,\kappa_x,\kappa_y}$ , can be rewritten in a simple way. Since we deal with low carrier

concentrations at which only the lowest LL is occupied, we can restrain ourselves to  $n = 0$ ,

$$\Delta E_{1,0} = E_{1,\kappa_x,\kappa_y} - E_{0,\kappa_x,\kappa_y} = \hbar\omega_c - \frac{4}{3} V_0 \beta^2 e^{-2\beta^2/3} b(\kappa_x, \kappa_y) \quad (5)$$

where  $b(\kappa_x, \kappa_y)$  denotes the curled bracket of Eq. (4).

The optical transition energy  $\Delta E_{1,0}$  enters the absorption probability  $\alpha(\omega)$  at a photon frequency  $\omega$ , see, e.g., Ref. 16, upon a transition between  $n = 0$  and  $n = 1$  LLs measured in our experiments

$$\alpha_{1,0} = \frac{2\pi}{\hbar} \int \frac{d^2\kappa}{(2\pi)^2} |\langle 1, \kappa_x, \kappa_y | p_x | 0, \kappa_x, \kappa_y \rangle|^2 \delta(\Delta E_{1,0} - \hbar\omega). \quad (6)$$

If we neglect the dipole transition matrix element for the moment, the characteristics spectral features corresponds to the van Hove singularities, see Fig. 5, in the the joint density of states (jDOS):

$$a(\omega) = \int \frac{d^2\kappa}{(2\pi)^2} \delta(\Delta E_{1,0} - \hbar\omega) f_{0,\kappa_x,\kappa_y} (1 - f_{1,\kappa_x,\kappa_y}),$$

in which all those transitions at a given energy  $\hbar\omega = \Delta E_{1,0}$  count where the initial ( $n = 0$ ) state is occupied and the final ( $n = 1$ ) state is empty, as expressed by the Fermi-Dirac occupation factors  $f$ . At a filling factor  $\nu = nh/eB = 2$ , which was assumed in Eq. (6),  $a(\omega)$  is a band of the width

$$w(B) = 6V_0\beta^2 e^{-2\beta^2/3} \quad (7)$$

situated close to  $\omega = \omega_c$ . The width of the band decreases with decreasing  $\nu$ , as the filling of the  $n = 0$  LL decreases and smaller portions of the magnetic Brillouin zone become available for transitions. In the limit of very large  $B$ ,  $a(\omega)$  turns into a delta-peak at exactly  $\omega = \omega_c$ .

Eq. (7) provides a reasonable basis for interpretation of experimental data presented in Figs. 3(a)-(c). The peak-to-peak distance shown as the lower data sets in Fig. 4 follows the magnetic field dependence of  $w(B)$  allowing to extract the values of  $V_0$  for the particular sample. It should be noted that the peak splitting observed in experiments probably does not correspond to the full width  $w$  as calculated using Eq. (7) because the lower edge of

Sample	$d_{\text{holes}}$	$d_{2\text{DEG}}$	$V_0$	$\zeta$
A	15-25	100	2.5 meV	2.4
B	20	100	3.5 meV	2.9
C	48	115	4 meV	4.0

TABLE I. Potential amplitude  $V_0$  and the corresponding dimensionless parameter  $\zeta$  for samples A, B and C as derived by fitting our data using Eq. (7), see text for details. The etching depths and the distances from 2DEG to the sample surface are also listed. Following relatively high  $\zeta$  values, the lattice parameter reduced down to  $a \approx 100$  nm would be more appropriate to achieve better defined Dirac cones for the given modulation strengths  $V_0$ , see Sec. II.

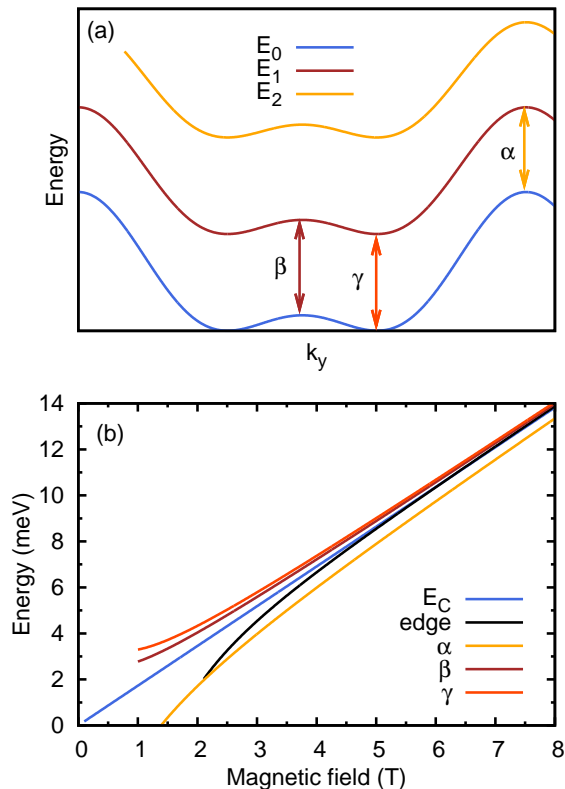


FIG. 5. (color online) Part (a): Schematic plot of three lowest lying LLs broadened into bands due to the lateral hexagonal modulation. Transitions originating in van Hove singularities in the joint density of states  $a(\omega)$  are marked by  $\alpha$ ,  $\beta$  and  $\gamma$ . Whereas  $\alpha$  and  $\gamma$  are the band edges,  $\beta$  is the logarithmic singularity corresponding to the saddle point between two neighbouring minima of  $\Delta E_{10}$  in  $\vec{k}$ -space (as shown in the top panel). Part (b): Magnetic field dependence of  $\alpha$ ,  $\beta$ ,  $\gamma$  jDOS singularities. “Edge” shows the lowest in energy allowed transition, as defined by the position of the Fermi level (for  $n = 5.0 \times 10^{10} \text{ cm}^{-2}$ ).  $E_c = \hbar\omega_c$  is the cyclotron energy.

the absorption band is suppressed for  $\nu < 2$  (this is the case of  $B > 2 \text{ T}$  and  $n < 10^{11} \text{ cm}^{-2}$ ).

However, other features of the absorption band also scale as  $cw(B)$ , where  $0 < c < 1$  is a constant. These features are shown in Fig. 5 and correspond to the indicated transitions of the broadened Landau bands  $E_{n,\kappa_x,\kappa_y}$ . The first states that become depopulated upon the filling factor dropping below two (that is when the magnetic field is increased) are those close to the top of the band. Hence, the transitions  $\alpha$  are the first ones to disappear from the absorption spectra. We note that the Zeeman splitting  $\varepsilon_z$  is roughly  $50\times$  lower than the LL broadening at  $B = 2 \text{ T}$ ,  $\varepsilon_z = ge\hbar/2m_0B \approx 0.05 \text{ meV}$ .

For the remaining two features  $\beta$  and  $\gamma$ , our form of the potential  $V(x, y)$  would imply  $c = 1/9$ . However, we believe that the feature  $\beta$  which leads to a logarithmic van Hove singularity in the jDOS, may be easily smeared out. Another candidate for an absorption feature is the

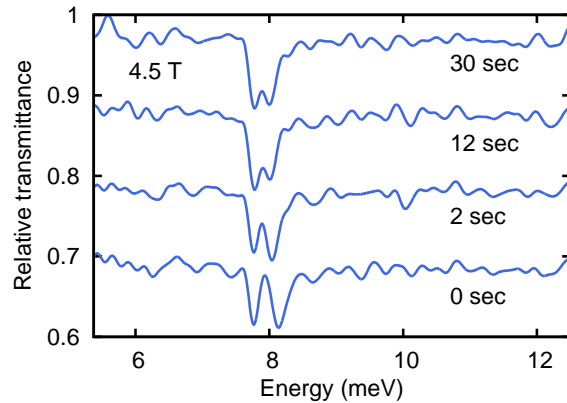


FIG. 6. (color online) Magneto-transmission spectra taken on the sample C at  $B = 4.5 \text{ T}$  and four different carrier concentrations. The density has been subsequently increased by exposing the sample to visible light for the indicated times. The spacing of observed modes clearly decreases with the carrier density. The spectra are shifted vertically for clarity.

Fermi edge (transitions from the states close to  $E_F$  to the next Landau band) which is also shown in the lower panel of Fig. 5. Although the Fermi edge does not precisely scale with  $w(B)$ , it always appears at frequencies  $\omega \approx \omega_c$  hence  $c \approx 1/3$ . The values of  $V_0$  inferred from fitting our data, assuming that the splitting of the CR mode corresponds to  $\frac{1}{3}w(B)$ , are shown in Tab. I alongside with the corresponding  $\zeta$ .

Splitting of the cyclotron peak in diminishing magnetic fields shown in Fig. 3 is also reminiscent of confined magneto-plasmons (CMP),<sup>17</sup> and this circumstance motivated us to perform a control experiment that excludes the effect of CMP, as described below. An infinite system with the 2DEG at zero magnetic fields can sustain plasma oscillations<sup>18</sup> of wavelength  $2\pi/q$  at frequency  $\omega_p(q) = \sqrt{e^2nq/2m^*\varepsilon_r\varepsilon_0}$ . Under the combined effect of the confinement and perpendicular magnetic field, the usual cyclotron resonance mode is experimentally found to shift from  $\omega_c$  to higher frequencies  $\sqrt{\omega_c^2 + \omega_p^2(q)}$ ; in a metallic stripe (quantum wire) of width  $W$ , the wavevector is given by  $q = \pi/W$  (see references in Sec. III of Ref. 20). Numerical simulations based on classical electrodynamics<sup>21</sup> in fact show a whole series of CMP peaks at frequencies  $\omega > \omega_c$  that correspond to integer multiples of the fundamental wave vector  $q = \pi/W$ .

Viewing our hexagonal modulation as (an array of) quantum wires with  $W = a$  is, of course, a bold approximation, nevertheless, it can provide us with a rough estimation of the energy of the lowest confined magneto-plasmon mode:

$$\omega_{CPM} = \sqrt{\omega_c^2 + \frac{\pi e^2 n}{2m^* a \varepsilon_r \varepsilon_0}} \approx \omega_c + \frac{\pi e n}{4Ba \varepsilon_r \varepsilon_0}. \quad (8)$$

Taking  $n \sim 2.5 \times 10^{10} \text{ cm}^{-2}$ , i.e., the carrier density three times smaller than estimated above, we can reproduce

our experimental data surprisingly well. Nevertheless, this agreement is probably only incidental, as the concept of magneto-plasmons fails to explain experimental data in Fig. 6. Here we, using external illumination, varied the electron density in the sample C and observed a clear decrease of the splitting of modes with the increasing carrier concentration, which directly contradicts Eq. (8). In addition, one does not expect  $\omega_{CMP}$  to change with the strength of the modulation, but just opposite behavior is clearly observed experimentally, see Fig. 4. We thus conclude that CMP do not underlie the observed splitting of the absorption peak.

## CONCLUSION

In conclusion, we stated four basic criteria that need to be met in order to achieve the proposed graphene-like bands in modulated semiconductor heterostructures, and thus earn them the name *artificial graphene*. Splitting of the cyclotron resonance line observed in far infrared magneto-optical experiments on laterally patterned samples allowed us to estimate the strength of the modulation potential. We found that the samples under study may be close to meeting criteria (i-iii) formulated in Section II and in order to comply also with criterion (iv), much lower magnetic fields ( $\sim 50$  mT) and preferably also somewhat lower temperatures (below 1 K) should be employed. This criterion does not seem to be fulfilled (magnetic fields too high) in the most recent experiments<sup>23</sup> thereby postponing still the first observation of Dirac fermion physics in artificial graphene to (possibly not too distant) future.

## ACKNOWLEDGEMENTS

The authors would like to sincerely thank P. Hubík and J. Čermák for technological assistance and J. Wunderlich for valuable critical remarks. Moreover, the sup-

port of the following institutions is acknowledged: the Ministry of Education of the Czech Republic projects LC510 and MSM0021620834, GAUK No. 250251, GACR No. P204/10/1020, the Academy of Sciences of the Czech Republic via Institutional Research Plan No. AV0Z10100521, GAAV contract KJB100100802, Fondation *NanoScience* via project Dispograph and Præmium Academiæ and last but not least, EC-EuroMagNetII under Contract No. 228043.

## Appendix A: Carrier concentration

*Theoretical estimates.* For the criterion (ii) to be met, the carrier concentration  $n$  must be adjusted appropriately to match the Fermi energies of the first and second Dirac cones. Taking Fig. 2(c) as an example,  $E_F - E_0 \approx 0.15$  and  $1.2$  meV, we estimate the carrier concentration quoted in the main text by  $n \approx (E_F - E_0)m^*/\pi\hbar^2$  where  $E_0 \approx -0.75$  meV is the bottom of the miniband structure. Strictly speaking, density of states belonging to the miniband structure will fluctuate around the free-2DEG value  $m^*/\pi\hbar^2$  but it will only lead to corrections of the desired  $n$  that are small compared to the precision with which we can estimate  $n$  experimentally.

*Experimental estimate.* We assume that the 2D electron gas is embedded in between two insulating GaAs layers with a refractive index of  $\tilde{n} \approx 3.0$  in the relevant spectral range. For a detector which is insensitive to polarization of radiation and high-quality sample ( $\omega_c\tau \gg 1$ ), the transmittance is given by  $T = \frac{1}{2}(|t_+|^2 + |t_-|^2)$ , where  $t_+ = 1/(1 + \sigma_+/2\tilde{n}\varepsilon_0c)$  and  $t_- \approx 1$ , see, e.g., Refs. 19 and 22. If we remain in the limit of weak absorption, we obtain the sample transmission:

$$T \approx 1 - \frac{\text{Re } \sigma_+}{2\tilde{n}\varepsilon_0c} = 1 - \frac{e^2n\tau}{2\tilde{n}\varepsilon_0cm^*} \frac{1}{1 + \tau^2(\omega - \omega_c)^2},$$

in terms of optical conductivity  $\sigma_+$ , which allows us to easily estimate the carrier density  $n$  in the studied samples.

\* nadvl@fzu.cz

<sup>1</sup> K. S. Novoselov, A. K. Geim, S. V. Morozov, D. Jiang, M. I. Katsnelson, I. V. Grigorieva, S. V. Dubonos, and A. A. Firsov *Nature* **438**, 197 (2005).

<sup>2</sup> A. K. Geim and K. S. Novoselov, *Nature Mat.* **6**, 183 (2007).

<sup>3</sup> B. Wunsch, F. Guinea, and F. Sols, *New J. Phys.* **10**, 103027 (2008).

<sup>4</sup> Ch.-H. Park, and S. G. Louie, *Nano Lett.* **9**, 1793 (2009).

<sup>5</sup> T. Ando, A. B Fowler, and F. Stern, *Rev. Mod. Phys.* **54**, 437 (1982).

<sup>6</sup> M. C. Geisler, S. Chowdhury, J. H. Smet, L. Höppel, V. Umansky, G. G. Gerhardtts, and K. von Klitzing, *Phys. Rev. B* **72**, 045320 (2005).

<sup>7</sup> S. Hugger, T. Heinzl, and T. Thurn-Albrecht, *Appl. Phys. Lett.* **93**, 102110 (2008).

<sup>8</sup> M. Gibertini, A. Singha, V. Pellegrini, M. Polini, G. Vignale, A. Pinczuk, L. N. Pfeiffer, and K. W. West, *Phys. Rev. B* **79**, 241406 (2009).

<sup>9</sup> M.S.-M. Dubois, Z. Zanolli, X. Declerck, and J.-C. Charlier, *Eur. Phys. J. B* **72**, 1–24 (2009).

<sup>10</sup> A. Rycerz, J. Tworzydło, and W. J. Beenakker, *Nature Phys.* **3**, 172 (2007).

<sup>11</sup> V. V. Cheianov, V. Fal'ko, and B. L. Altshuler, *Science* **315**, 1252 (2007).

<sup>12</sup> J.-L. Garcia-Pomar, A. Cortijo, and M. Nieto-Vesperinas, *Phys. Rev. Lett.* **100**, 236801 (2008).

- <sup>13</sup> G. De Simoni, A. Singha, M. Gibertini, B. Karmakar, M. Polini, V. Piazza, L. N. Pfeiffer, K. W. West, F. Beltram, and V. Pellegrini, *Appl. Phys. Lett.* **97**, 132113 (2010).
- <sup>14</sup> X. F. Wang, P. Vasilopoulos, and F. M. Peeters, *Phys. Rev. B* **69**, 035331 (2004).
- <sup>15</sup> I. S. Gradshteyn and I. M. Ryzhik, *Table of Integrals, Series, and Products*, Academic, New York, (1980).
- <sup>16</sup> V. Y. Demikhovskii and A. A. Perov, *J. of Exp. and Theor. Phys.* **87**, 973 (1998).
- <sup>17</sup> O. M. Fedorych, S. A. Studenikin, S. Moreau, M. Potemski, T. Saku, and Y. Hirayama, *Int. J. of Mod. Phys. B* **23**, 2698 (2009).
- <sup>18</sup> F. Stern, *Phys. Rev. Lett.* **18**, 14 (1967).
- <sup>19</sup> K. W. Chiu and T. K. Lee, *Surface Science* **58**, 182–184 (1976).
- <sup>20</sup> S. A. Mikhailov, *Phys. Rev. B* **70**, 165311 (2004).
- <sup>21</sup> S. A. Mikhailov and N. A. Savostianova, *Phys. Rev. B* **71**, 035320 (2005).
- <sup>22</sup> M. L. Sadowski, G. Martinez, M. Potemski, C. Berger, and W. A. de Heer, *Int. J. Mod. Phys. B* **21**, 1145 (2007).
- <sup>23</sup> G. de Simoni, A. Singha, M. Gibertini, B. Karmakar, M. Polini, V. Piazza, L. N. Pfeiffer, K. W. West, F. Beltram, and V. Pellegrini, *Appl. Phys. Lett.* **97**, 132113 (2010).